Pergamon

*Int. J. Multiphase Flow* Vol. 23, No. 5, pp. 815–829, 1997

Printed in Great Britain
PII: S0301-9322(97)00020-7
0301-9322/97 $17.00 + 0.00

# VOID FRACTION MEASUREMENTS IN GAS–LIQUID FLOWS UNDER $1-g$ AND $\mu-g$ CONDITIONS USING CAPACITANCE SENSORS

K. J. ELKOW and K. S. REZKALLAH
Department of Mechanical Engineering, University of Saskatchewan, Saskatoon, Canada S7N 5A9

*(Received 21 February 1996; in revised form 28 February 1997)*

**Abstract**—Capacitance void fraction sensors were used to obtain void fraction measurements in vertical two-phase water-air flow in a small diameter tube (9.53 mm). Measurements were obtained at $1-g$ and $\mu-g$ conditions. Comparisons were made between the void fraction values obtained at both gravity conditions by matching the flow rates obtained at $\mu-g$ conditions. It was found that the average void fraction values were comparable for the bubble, transitional flow (slug–annular flow at $\mu-g$, and churn flow at $1-g$), and annular flow regimes. The slug flow regime showed a slightly higher overall average of about 10% at $\mu-g$ conditions. The distribution coefficient, $C_0$, which takes into account the flow regime and the void fraction profile was found to be 1.25 for bubble and slug flows at $\mu-g$, and 0.61 and 1.17 for $1-g$ bubble and slug flows, respectively. This suggests that a 'flatter' void fraction profile exists for slug flow at $1-g$ as compared to $\mu-g$. The value of 0.61 for bubble flow agrees well with the typical values obtained by averaging the 'saddle' shape void fraction profile typically seen at $1-g$.


*Key Words:* two-phase flow, void fraction, capacitance sensor, microgravity

## 1. INTRODUCTION

In the past 5 decades, extensive data sets were collected on ground for two-phase gas–liquid flows (both adiabatic and in boiling/condensation) in horizontal, vertical, and inclined channels. Due to a limited access to the space environment and the high cost associated with conducting research at $\mu-g$ (microgravity, $ms^{-2}$), the available data for $\mu-g$ two-phase flow is still sparse. Terrestrial applications for two-phase flow include flow refrigerants in heat exchanger systems, cooling of nuclear reactors, petro-chemical industries, chemical processes and in power plants. Some of the aerospace applications include boiling and condensation in channels of heat removal devices, thermal-hydraulic power cycles for space stations and large satellites, and in the transfer and storage of cryogenics. An experimental approach is needed to provide the bench mark data for accurate modeling and optimum design of equipment where two-phase flow occurs.

Due to the transient nature of two-phase flows, most analysis techniques involve an ensemble average that is obtained from various data taken at the same flow conditions, or by applying a time-average over data from a single recording. Some of the common techniques for obtaining void fraction measurements include gamma-ray attenuation, conductance probes, quick-closing valves, and capacitance methods. The selection of any of these methods largely depends on its application, and whether a volumetric average or a local void fraction measurement is desired. A capacitance sensor provides a non-intrusive way to measure void fraction. It can be used to obtain time-averaged void fraction measurements, and its time varying output signal can be also used as a flow pattern identifier. Research using capacitance measurements include those by Li *et al.* (1992), Albouelwafa and Kendall (1979), Shu *et al.* (1982), and Masuda *et al.* (1980).

Some of the more recent work which involved the measurement of void fraction at reduced gravity was done by Bousman (1995). He used air–water, air–water/glycerin (50% by weight) and air–water/zonyl FSP mixtures flowing in 12.7 and 25.4 mm, i.d. tubes. The air–water results are later compared to those obtained in this study.

An experimental study by Grossetête (1995) involved an investigation into the development of void fraction and velocity profiles for bubble flow in a 38 mm, i.d. vertical tube on ground.

Water–air mixtures were used and local measurements were taken with a dual-fiber optical probe and a hot film sensing probe at three $L/D$ (length/diameter) locations. It was noted that as the $L/D$ ratio increased, the high void fraction values at the wall diminished with an increasing gas concentration near the center of the tube. These results are discussed later in this paper.

## 2. EXPERIMENTAL EQUIPMENT

A schematic of the flight apparatus can be seen in figure 1. The main objective in designing the flight apparatus was to simultaneously obtain pressure drop, heat transfer and void fraction measurements for two-phase adiabatic flow as well as to obtain high speed video recordings. Data was collected at simulated near weightlessness by flying the equipment on NASA's KC-135 zero-gravity airplane. Data was also taken at $1 - g$ (earth's gravity = 9.81 m/s$^2$) prior to and after each flight. The major hardware components consisted of a closed liquid loop and an open gas loop. A 486/66 MHz computer was used in the Data Acquisition and Control System (DAS).

The flight apparatus has a vertical test section where pressure, void fraction, and temperatures are measured. In addition, there are vertical and horizontal flow observation sections where video recordings are made. The test section tube has an inside diameter of 9.53 mm. A variable speed pump/separator unit moves the single-phase liquid through a heat exchanger. The liquid then enters any combination of four venturies which were manually selected to control the flow. Following the venturies, the liquid is measured with a turbine flow meter before entering the mixer. At the mixer the flow was directed upwardly. The air injector at the mixer is located 0.142 m from

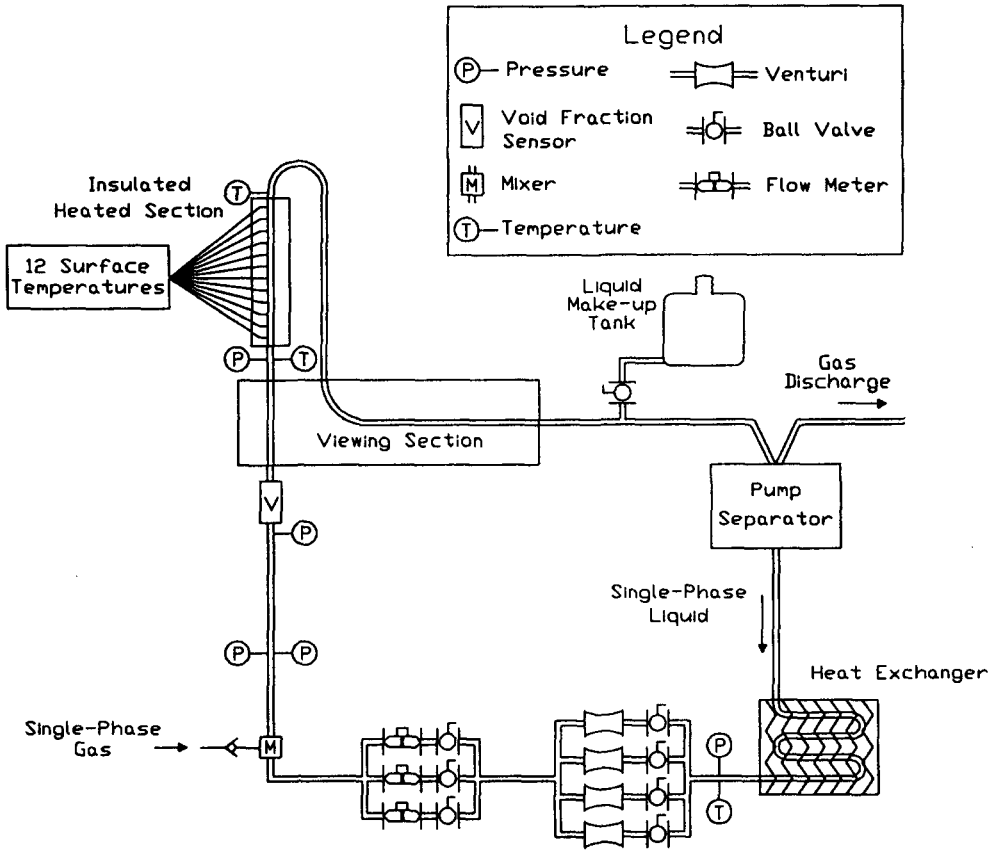


Figure 1. Schematic of the flight apparatus flown on the KC-135.

the base of the vertical test section. The first pressure taps, where absolute and gauge pressures are recorded, are located 0.281 m from the mixer ($L/D = 29.5$). A middle pressure (gauge) tap was located further downstream at 0.586 m from the mixer ($L/D = 61.5$). The inlet port of the void

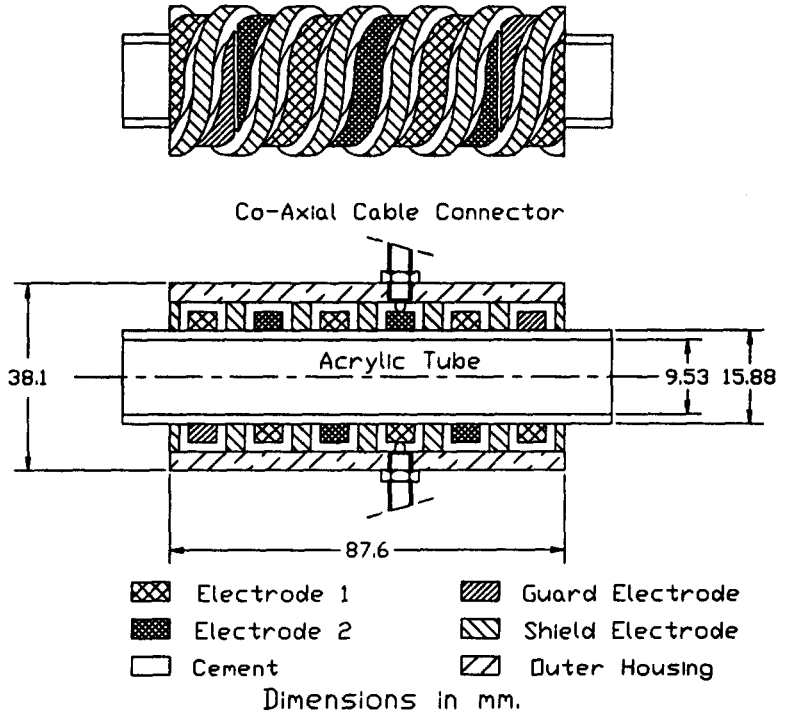


(a)

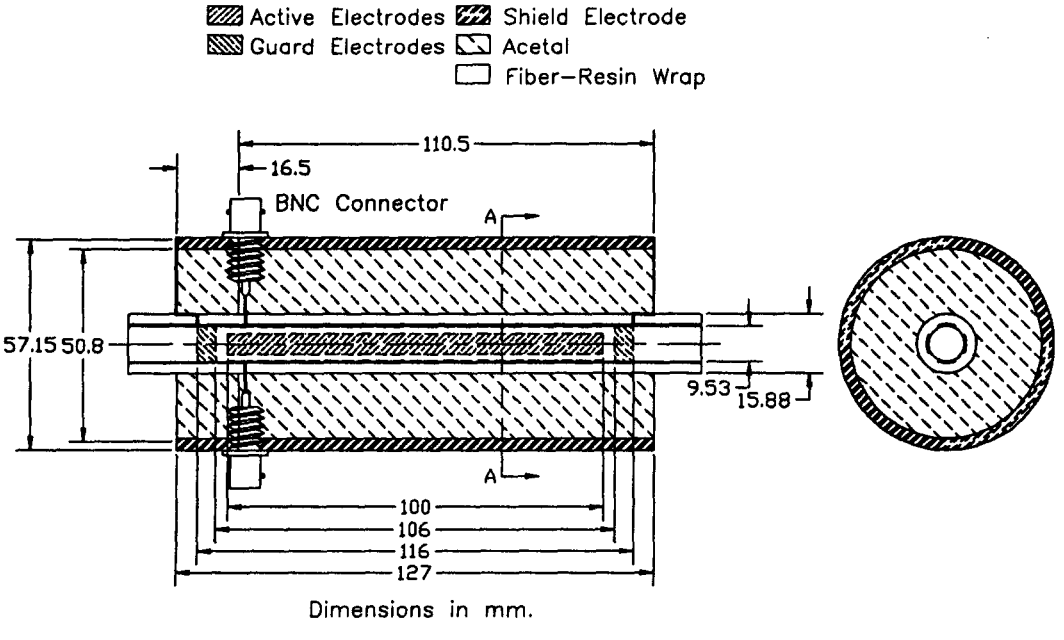


(b)

Figure 2. Schematics of the (a) helical, and (b) concave plate capacitance void fraction sensors.

fraction sensor is 0.62 m downstream from the mixer ($L/D = 65.1$), and the top pressure (gauge) tap is 0.974 m downstream from the mixer ($L/D = 102.3$). Just below the top pressure tap is a vertical viewing section that is 0.127 m long. The viewing section is made of acrylic and filled with glycol. Glycol is selected since its index of refraction and that of acrylic are similar, (1.47 and 1.49, respectively), providing clearer images. The flow then passes through a heated test section (1.05 m from the mixer, $L/D = 110$), and then through a horizontal viewing section before returning to the pump/separator. At the pump/separator, air is vented overboard while the liquid is re-circulated. A make-up liquid tank ensured sufficient supply of liquid to the loop.

For the ground tests, filtered air was supplied from an air compressor. During the flights, air was supplied from cylinders of compressed air, approximately 15.2 MPa and regulated down to 689.5 kPa before it passed through the mass flow controller. The air was then injected into the flow at the mixer through small holes around its periphery. The liquid flowed through the center of the mixer and gas was uniformly mixed with the liquid through the small holes. The two-phase flow continued through the flow loop and returned to the pump/separator.

The liquid flow rate was measured using two OMEGA© turbine flow meters having a range of 0.3–9 LPM (liters per min); giving $U_{SL} = 0.07$–$2.1$ m/s, and the other 0.5–15 LPM ($U_{SL} = 0.12$–$3.5$ m/s). For air flow measurements, two computer controlled mass flow controllers were used; 0–20 SLM (standard liters per min) and 0–100 SLM ranges. Absolute pressure was measured with a Validyne 0–414 kPa pressure transducer. Three differential gauge pressures were also measured with Validyne pressure transducers having diaphragm ranges of $\pm 14$ kPa and $\pm 21$ kPa. A NAC Color HighSpeed Video (HSV 1000) set at 1000 frames per s, was used to record the two-phase flow patterns. The gravity level measurements were taken with onboard accelerometers which were provided by the Canadian Space Agency.

## 3. SENSOR DESIGN AND CALIBRATION

Two capacitance sensors, shown in figure 2, were used to collect void fraction data, one having helical wound electrodes and the other having concave plate electrodes. A detailed discussion of the sensors can be found in Elkow and Rezkallah (1996).

The helical wound electrode sensor was 88 mm long. The pitch of the helix was 29.2 mm and the electrode width was 3.58 mm. A brass electrical shield was placed over the electrodes to

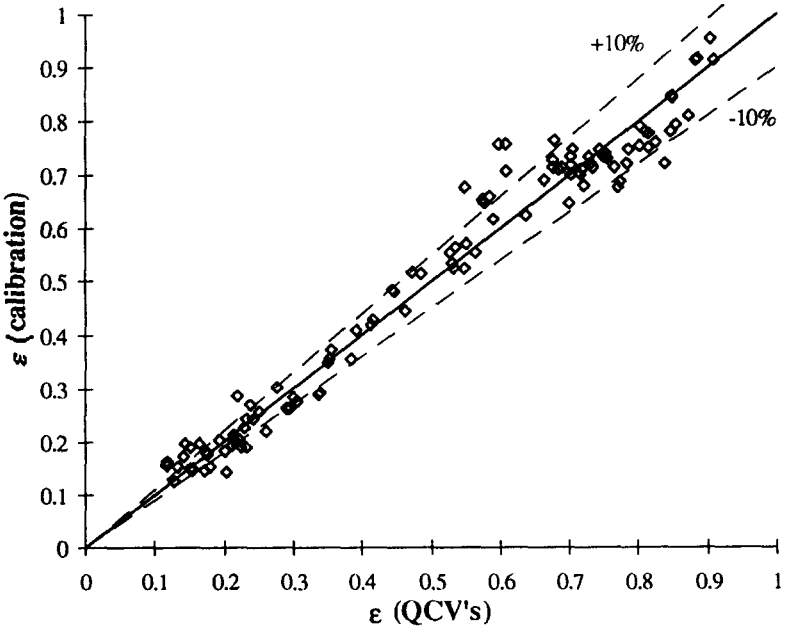


Figure 3. Calibrated void fraction for the helical plate capacitance sensor as a function of the void fraction trapped between two QCVs.

eliminate stray capacitance. Electronics for this sensor were based on a charge/discharge principle, operating at 2 MHz, as discussed by Huang *et al.* (1988). The time response of the measuring circuit has a time constant of 10 $\mu$s, corresponding to a dynamic response of 100 kHz.

The concave plate capacitor had four electrodes, 100 mm long and 5.51 mm wide, each having a 60° arc length. A brass outer shield was placed over the entire electrode configuration to protect them from stray capacitance. Two electrodes, opposite from each other were used for measurements; the other two were grounded to an outer shield. A HP 4284A impedance meter, operating at an excitation frequency of 1 MHz was used to obtain measurements.

A signal analysis of the sensor's output was conducted to ensure that there was a good signal-to-noise ratio and that aliasing was not present (aliasing occurs when a signal is improperly represented by another). This can occur when the sample rate is too low resulting in an improper representation of the input signal. Tests were conducted using a TEAC FM data recorder at both 1024 and 2048 Hz. From the FFT plots it was found that a sample rate of 70 Hz would ensure a non-aliased signal.

Calibration of the sensors was conducted using de-ionized and distilled water. The sensors were placed in a vertical calibration loop where electrically triggered, quick-closing valves were used to trap two-phase flow in a test section 1.592 m long. Details of the calibration can be found in Elkow and Rezkallah (1996).

In summary, the superficial liquid velocities were 0.1, 0.33, 0.6, 1.0, 1.7, 2.4 and 3.3 m/s. The air flow was varied such that the widest range of void fraction could be obtained. Since the output from the helical sensor was nonlinear, a curve fit was applied to the data relating the void fraction trapped between the valves, the voltage output of the sensor, and the above mentioned superficial liquid velocities. Results of the calibration for the helical plate capacitor are shown in figure 3. It can be seen that most of the data fall within $\pm 10\%$ of the actual values. Using linear regression, the standard error was 0.046. There is slightly more scatter at a void fraction around 0.7 as compared with other void fraction values. This scatter is in the churn flow regime which is highly oscillatory due to the alternating 'competition' between the forces of gravity pulling the fluid downward and those due to the inertia of the gas holding the fluid upwards.

The calibration results for the concave plate capacitor are shown in figure 4. By applying a linear regression to the data, (represented by the solid line), the correlation coefficient squared, $R^2$, was found to be 0.96. The dashed lines represent a fit standard error of 0.05. Measurement uncertainty of the readings for the concave plate and helical wound sensors were 0.7 and 5% of full scale, respectively.

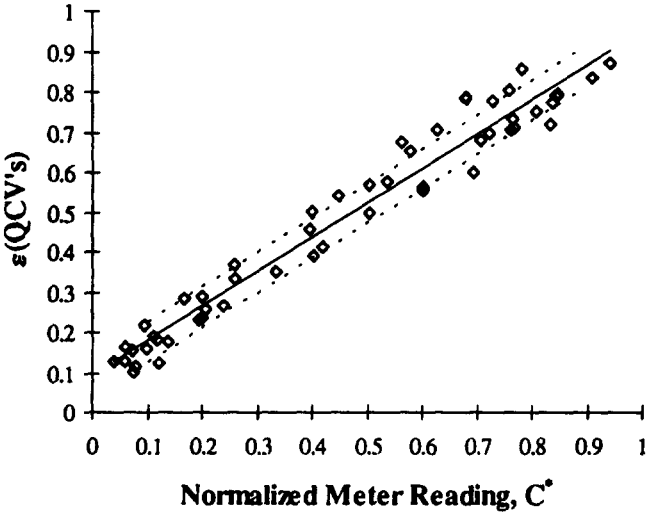


Figure 4. Calibration of the concave plate capacitance sensor using the HP 4284A impedance meter.

## 4. FLIGHT AND GROUND RESULTS

In February 1994, data for two-phase water–air flow was collected during low gravity periods onboard NASA's KC-135 aircraft. Five separate flights were conducted where pressure drop, heat transfer and void fraction data were measured simultaneously. A total of 61 data points were

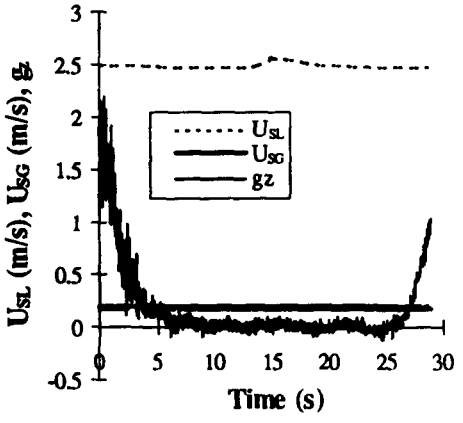


**(a) Typical plot of $g_z$ and flow settings.**

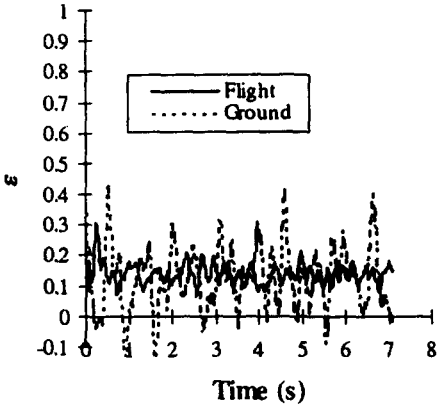


**(b) Time trace for bubble flow.**

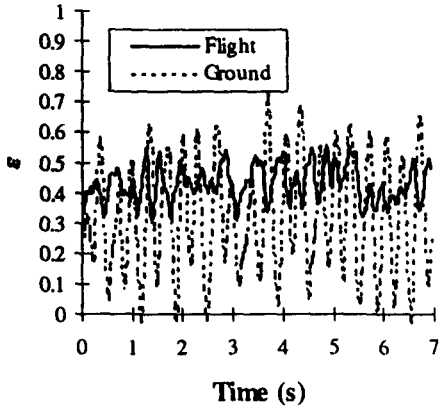


**(c) Time trace for slug flow.**

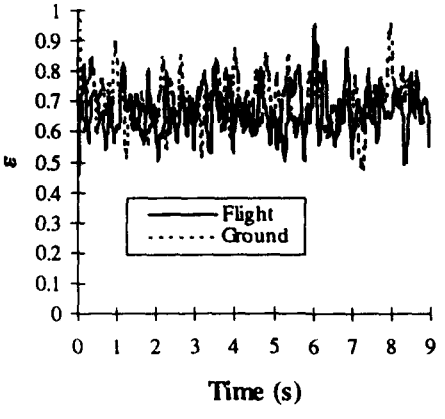


**(d) Time trace for transitional flow.**

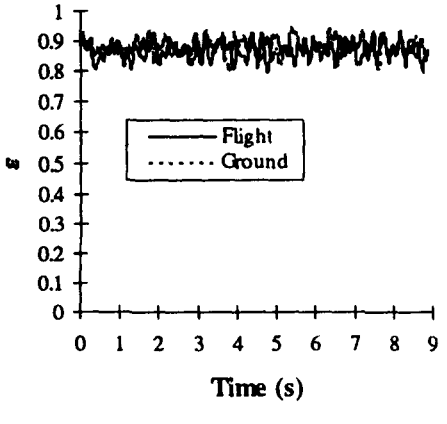


**(e) Time trace for annular flow.**

Figure 5. Plots of (a) typical profile of normalized gravity level and superficial liquid and gas velocities, and (b)–(e) void fraction signals.

used in the void fraction analysis. Superficial liquid flow settings from 0.07 to 2.5 m/s, and superficial gas velocities in the range of 0.1–18 m/s were tested during those flights. Void fractions from 0.1 to 0.9 covering the total range from bubble to annular flow regimes, were obtained. Flight data was selected where the normalized gravity level, $g_z$, was $\pm 0.04$. Typical superficial liquid and gas settings as well as the normalized gravity level during a low gravity period can be seen in figure 5(a). Ground data at approximately the same flow settings as those obtained during the flight tests were obtained prior to and after the flights for the sake of comparisons. A helical plate capacitance sensor was used in both flight and ground runs.

The ground data using the two capacitance sensors are presented in terms of the measured void fraction as a function of the 'pseudo' void fraction ratio $U_{SG}/U_{SL}$ (superficial gas velocity/superficial liquid velocity); these are shown in figure 6. It can be seen that the scatter in the bubble and churn flow regimes is much less with the concave plate sensor. However, the RMS deviation between the two readings is within 1.4–6% (being highest in the churn flow regime). Figure 7 shows the average void fraction data sets obtained during both flight and ground tests as a function of the 'pseudo' void fraction ratio, $U_{SG}/U_{SL}$. Further comparisons for each flow regime were made between ground and flight data by matching the ratios of $U_{SG}/U_{SL}$. Only the data points which had similar values for $U_{SG}/U_{SL}$ were used in the comparisons here. In general, the percent difference in the ratio of $U_{SG}/U_{SL}$ for the flight and ground data is within approximately $\pm 3$–4%. However, due to the limited number of data points in the annular flow regime, the percent difference is higher. It was found that the average void fraction values for bubble, transitional and annular flows were comparable for both flight and ground data, with slug flow at $\mu - g$ being approximately 9–10% higher than the $1 - g$ values. Typical time trace of the void fraction for these regimes can be seen in figure 5(b)–(e). Tabulated data showing the flow settings and gravity levels for figure 5(b)–(e) are listed in table 1.

Since two-phase flow measurements are strongly flow regime dependent, more informative comparisons should be made for each flow regime individually. The results of these comparisons are shown in figures 8–11 for bubble, slug, transitional, and annular flows, respectively.

Data for the bubble flow regime is shown in figure 8. For a pseudo void fraction ratio below approximately 0.1, the results show a tendency for the flight data to be approximately 8–25% higher than those taken at $1 - g$. Above $U_{SG}/U_{SL} = 0.1$, the difference is reduced until the trend

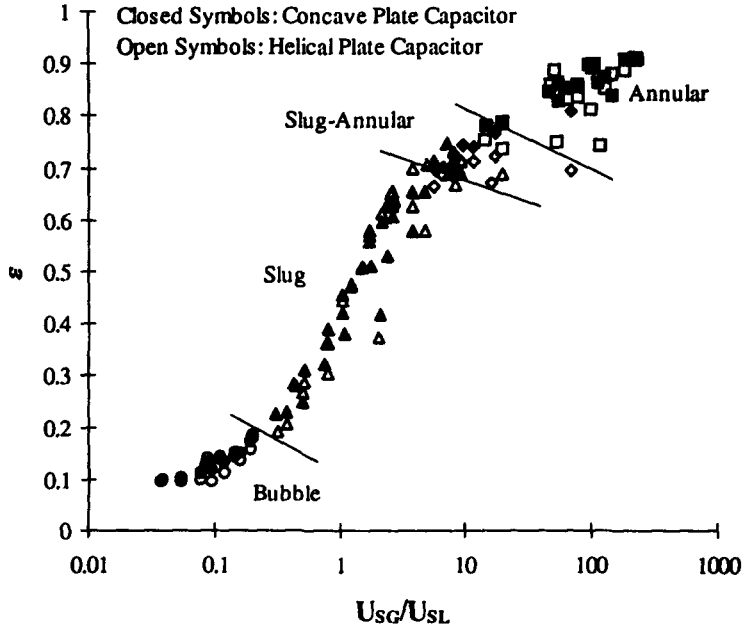


Figure 6. Comparison of ground data from the helical and concave plate capacitance sensors.

Table 1. Data obtained from the flight and ground test showing flow rates, gravity level, average void fraction, and flow regimes

| Flight/ground parabola | $U_{SL}$ (m/s) | $U_{SG}$ (m/s) | Normalized gravity $g_z$ | Average $\epsilon$ | Flow regime |
|---|---|---|---|---|---|
| 94F3P22 | 0.86 | 0.09 | −0.042 | 0.139 | Bubble |
| 94F3P13 | 0.24 | 0.19 | −0.003 | 0.437 | Slug |
| 94F5P16 | 0.39 | 6.97 | 0.007 | 0.682 | Slug–Annular |
| 94F5P9 | 0.07 | 13.9 | 0.022 | 0.875 | Annular |
| 94G3P22 | 0.84 | 0.09 | 1.0 | 0.141 | Bubble |
| 94G3P13 | 0.24 | 0.19 | 1.0 | 0.363 | Slug |
| 94G5P16 | 0.40 | 6.92 | 1.0 | 0.721 | Churn |
| 94G5P9 | 0.07 | 13.9 | 1.0 | 0.887 | Annular |

is reversed with the $1-g$ data slightly higher than the $\mu-g$ counterpart (approximately 7–16% higher). The higher void fraction ($\epsilon$) at $\mu-g$, where $\epsilon < 0.2$ and $U_{SG}/U_{SL} \leqslant 0.1$, can be attributed to the significant reduction in slip between the phases, combined with an increased influence of surface tension under reduced gravity. These changes lead to the bubbles being able to sustain their shape even at high gas content, while the rate of collision and coalescence of the bubbles is significantly reduced.

The slug flow results are shown in figure 9. For this regime, the void fraction appears to be consistently higher for the $\mu-g$ data, with a difference that ranges from 3% to 35%, with an overall average of approximately 10%. This trend seems to be consistent up to a void fraction of approximately 0.70 beyond which the percent difference in void fraction decreases. This occurs near the transition to slug-annular flow at $\mu-g$, and churn flow at $1-g$. In the latter, flow reversal is observed and could greatly influence the void fraction readings in that region.

The results for transitional flows (slug–annular flow at $\mu-g$, and churn flow at $1-g$) are shown in figure 10. The average values of void fractions in this transitional region are comparable for both the $\mu-g$ and $1-g$ cases. As mentioned earlier, the slug–annular flow is in a transition where inertia forces are becoming more dominant than those due to surface tension. The liquid slugs at these conditions contain a highly aerated frothy mixture, which could in turn cause large fluctuations in the void fraction measurements.

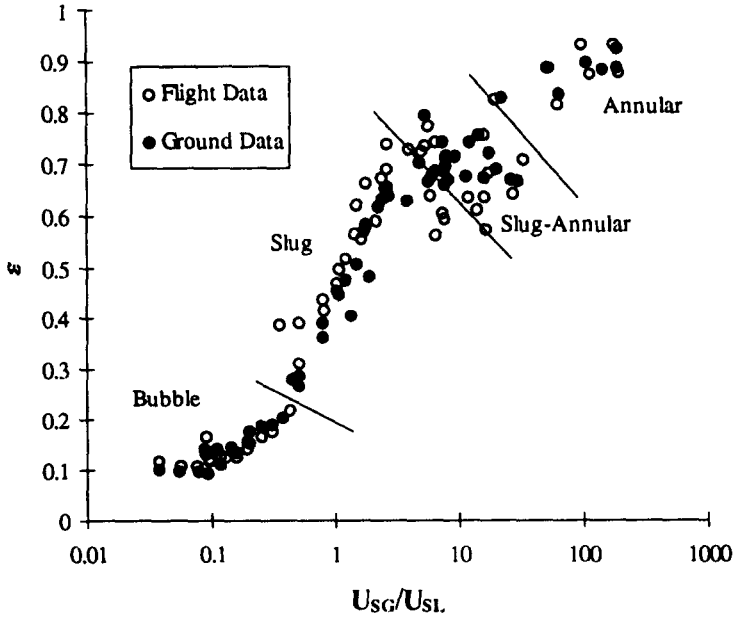


Figure 7. Flight and ground void fraction data.

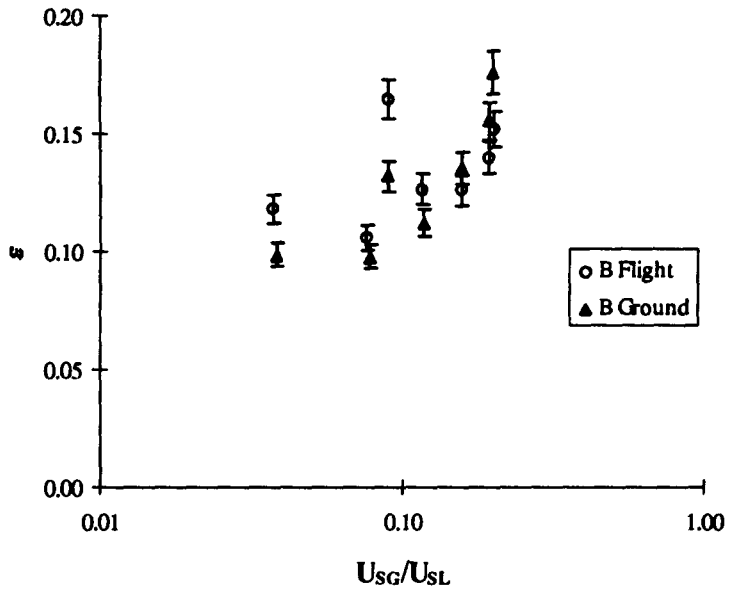


Figure 8. Comparison of the bubble flow regime, (B), for the flight and ground data.

Finally, the results for annular flow are shown in figure 11. The annular flow results show that the $\mu - g$ and $1 - g$ data are very similar. This is expected since, under both $1 - g$ and $\mu - g$ conditions, the flow is highly turbulent and inertia forces are dominant in both cases. The difference between the $1 - g$ and $\mu - g$ void fraction values is within $\pm 5\%$.

Another comparison was made with the $\mu - g$ data collected by Bousman (1995). The $\mu - g$ void fraction data collected during the present study and those of Bousman (1995) are plotted in figure 12 in terms of the volumetric gas quality, $\beta$, as a function of the measured void fraction,

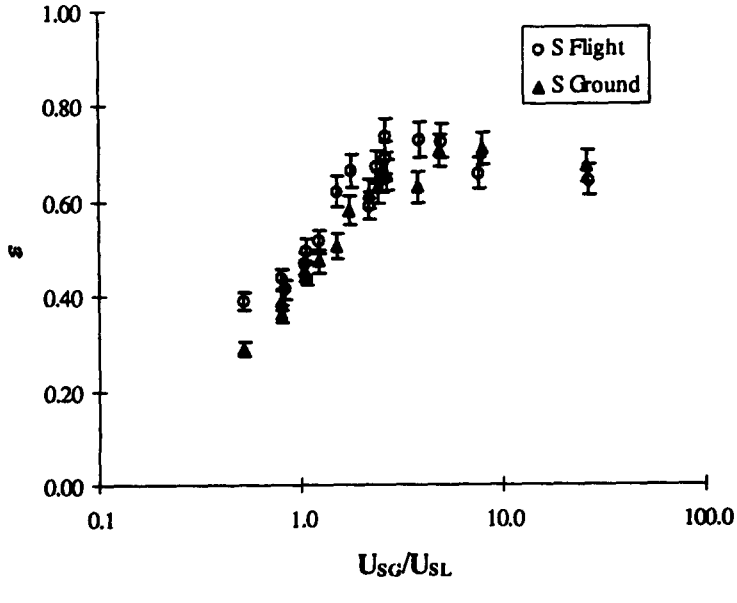


Figure 9. Comparison of the slug flow regime, (S), for the flight and ground data.

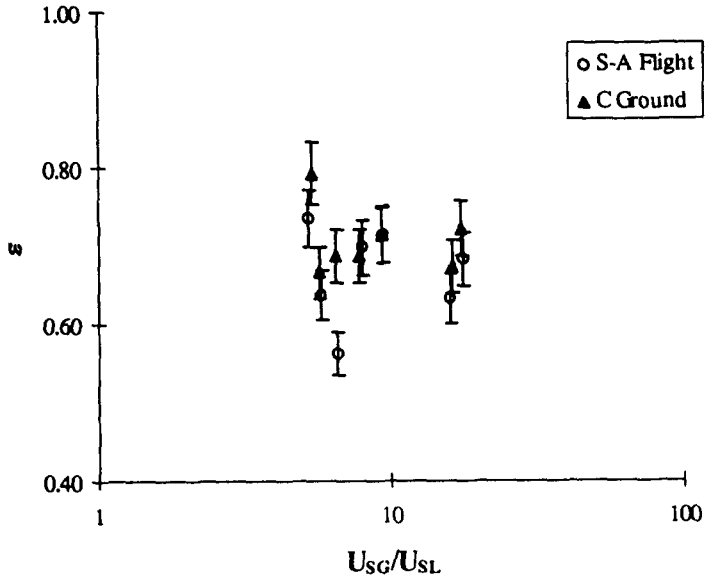


Figure 10. Comparison of the slug–annular flow regime, (S–A), at $\mu - g$ and the churn flow regime, (C), at $1 - g$.

$\epsilon$, where $\beta$ is defined as

$$\beta = \frac{Q_G}{(Q_G + Q_L)} = \frac{U_{SG}}{(U_{SG} + U_{SL})}. \quad [1]$$

This is a convenient parameter to use in situations where the reported data in the literature are in terms of $U_{SL}$ and $U_{SG}$.

Bousman's $\mu - g$ data was collected for horizontal flow in 12.7 and 25.4 mm, i.d. tubes aboard NASA's KC-135 aircraft using an impedance method (two parallel wires were located in the flow path, spanning the cross section of the tube). The wires were separated by 2.5 mm, and the void fraction was determined by measuring the electrical conductance between the wires. Uncertainty

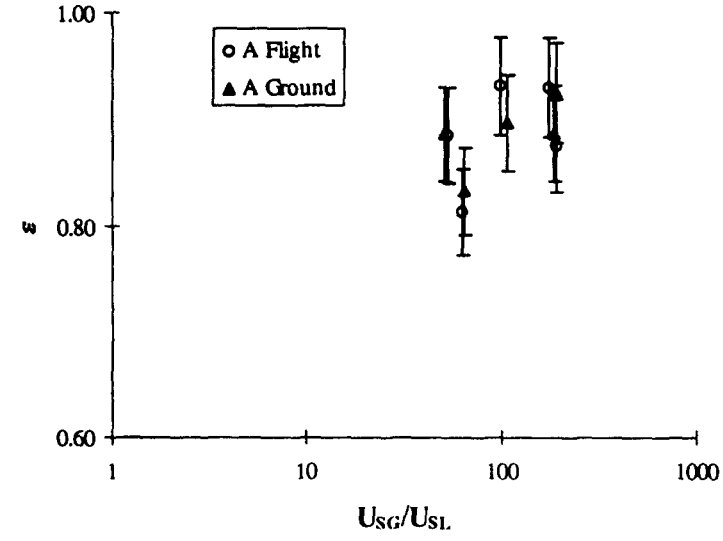


Figure 11. Comparison of the annular flow regime, (A), for the flight and ground data.

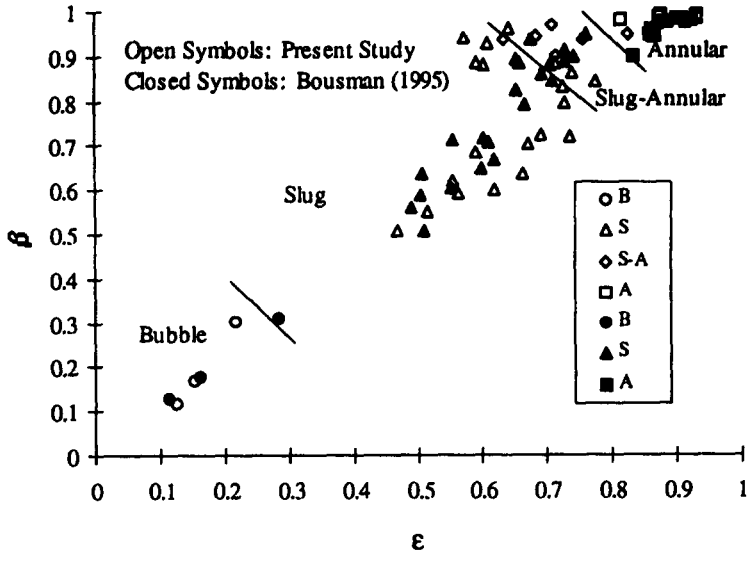


Figure 12. Comparison between the present study and Bousman (1995) at $\mu - g$ conditions.

in the void fraction measurements made by Bousman (1995) was reported to be $\pm 0.65\%$ in the void fraction range between $0 < \epsilon < 0.75$. Void fraction data was reported for only the 12.7 mm, i.d. tube.

The comparison between the present data points and those of Bousman (1995) was done by matching $\beta$ for each flow regime. As seen in table 2, $\beta$ was matched within $\pm 3\%$, except for bubble flow ($\pm 8\%$). It should be noted that in Bousman's (1995) reported void fraction data, none of the set points were classified as slug–annular flow. Therefore, the comparison of slug–annular flow shown in table 2 is based on similar values of $\beta$ that were classified as slug–annular flow in the present study. The classification of the slug–annular flow, particularly at $\mu - g$ where this transition occurs over a much wider range of liquid and gas velocities, is very difficult resulting in some discrepancies between researchers. This could perhaps explain the large RMS difference between the two sets of data in this region ($\pm 15.3\%$), compared to the average of $\pm 7.9\%$. In the present study, however, visual images of the flow were substantiated with signal analysis from the void fraction sensor.

## 5. VOID FRACTION DISTRIBUTION COEFFICIENT

Since under most practical conditions the two phases may not travel at the same velocity, consideration must be given to the relative velocity between the two phases. Starting with the continuity equations for both phases, Zuber and Findlay (1965) developed a general expression for predicting the average void fraction which takes into account the relative velocity between the two phases and the void fraction profile across the tube. The expression is given as

$$\frac{\langle \beta \rangle}{\langle \epsilon \rangle} = C_0 + \frac{\langle \epsilon u_{Gj} \rangle}{\langle \epsilon \rangle \langle j \rangle}, \qquad [2]$$

Table 2. Comparison between the present study and data from Bousman (1995)

| Flow regime | Average percentage difference in $\beta$ | RMS of $\epsilon$ (%) |
|---|---|---|
| Bubble | $\pm 8$ | $\pm 3.8$ |
| Slug | $\pm 3$ | $\pm 8.1$ |
| Slug–Annular | $\pm 1$ | $\pm 15.3$ |
| Annular | $\pm 1.5$ | $\pm 4.3$ |
| Average | $\pm 3.4$ | $\pm 7.9$ |

Table 3. The effect of $\epsilon_w$ and $\epsilon_c$ on $C_0$

| Case 1 | Case 2 | Case 3 |
|---|---|---|
| $\epsilon_c < \epsilon_w$ | $\epsilon_w = \epsilon_c = \epsilon$ | $\epsilon_c > \epsilon_w$ |
| $C_0 < 1$ | $C_0 = 1$ | $C_0 > 1$ |

where $u_{Gj}$ is the drift velocity of the gas relative to the mean fluid velocity and $j$ is the volumetric flux, i.e. $j = U_{SG} + U_{SL}$, and $\langle\rangle$ represents the average value of the term within the brackets. The constant $C_0$ is known as the 'distribution coefficient' (more on this constant will be presented later). The second term on the right-hand side of [2] is the weighted mean drift velocity which takes into account the local relative velocity. Expressions for the weighted drift velocity of the gas with respect to the mean fluid were also given by Zuber and Findlay (1965) as

$$\frac{\langle \epsilon u_{Gj} \rangle}{\langle \epsilon \rangle} = 1.53 \left[ \frac{\sigma g \Delta \rho}{\rho_L^2} \right]^{\frac{1}{4}}, \qquad [3]$$

for bubbly flow; and

$$\frac{\langle \epsilon u_{Gj} \rangle}{\langle \epsilon \rangle} = 0.35 \left[ \frac{g \Delta \rho D}{\rho_L} \right]^{\frac{1}{2}} \qquad [4]$$

for slug flow (where $\rho$ is density). Equations [3] and [4] were developed based on analysis where the drift velocity, $u_{Gj}$, was equated to the terminal velocity of a particle rising in an infinite medium.

Equation [2] is in a general form that could be applied to any flow regime to predict the void fraction. Since the phase velocities and the void fraction profiles (as well as the relative velocities between the phases) are taken into account, this equation is of a general use. The distribution coefficient, $C_0$, accounts for the non-uniform distribution of the void fraction over the cross section of the tube, and is obtained from:

$$C_0 = \frac{\langle \epsilon j \rangle}{\langle \epsilon \rangle \langle j \rangle}. \qquad [5]$$

The distribution coefficient, $C_0$, depends on both the flow regime and the void fraction profile. Depending on the radial void fraction distribution, $C_0$ can be greater, equal to, or less than one. These conditions are summarized in table 3, where $\epsilon_c$ is the void fraction at the center of the tube, and $\epsilon_w$ is the void fraction at the wall.

## 6. COMPARISONS OF THE DISTRIBUTION COEFFICIENT

It should be noted that the results in this section have been obtained, and are presented for two capacitance sensors. The capacitance sensor which was flown in February 1994 was a helical wound electrode sensor. Ground data, on the other hand, was collected with both the helical and a concave plate sensor that was later designed and calibrated, Elkow (1996). The flow settings were matched to those obtained during flight tests.

Equation [2] was applied to both the ground and flight data. It has been already stated that due to the low gravity levels during the periods of $\mu - g$, buoyancy effects would be minimized and thus, the second term on the right-hand side of [2] can be neglected. Therefore, by plotting $\beta$ as a function of $\epsilon$, as shown in figure 13, $C_0$ was found by linear regression to be 1.25 for the $\mu - g$ data in the bubble and slug flow regimes.

The results for slug flow at $1 - g$ are shown in figure 14. From linear regression, $C_0$ was found to be 1.17 and $\langle \epsilon u_{Gj} \rangle / \langle \epsilon \rangle = 0.03$. Using [4] for slug flow, where the properties of water were evaluated at the average temperature of 30°C, a value of 0.107 was obtained for $\langle \epsilon u_{Gj} \rangle / \langle \epsilon \rangle$. Thus, the distribution parameter, $C_0$, for $\mu - g$ bubble and slug flow, and $1 - g$ slug flow are 1.25 and 1.17, respectively. For water–air flow at $\mu - g$, Bousman (1995) obtained a $C_0$ value of 1.27, which is in very good agreement with the present data considering that independent measurements were made using different sensor's geometry.

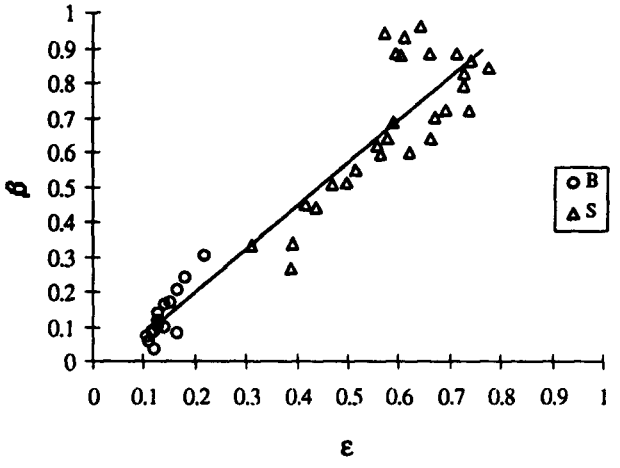


Figure 13. $\beta$ as a function of $\epsilon$ for bubble and slug flow at $\mu - g$, $C_0 = 1.25$.

The bubbly flow results plotted in terms of the actual gas velocity, $u_G$, as a function of the total volumetric flux, $U_{SG} + U_{SL}$, can be seen in figure 15. From linear regression, $C_0$ was found to be 0.61 and $\langle \epsilon u_{Gj} \rangle / \langle \epsilon \rangle = 0.19$. As seen earlier, $C_0 < 1.0$ occurs when $\epsilon_c < \epsilon_w$. The typical 'saddle' shape profile is seen where the void fraction is higher at the wall of the tube and drops off towards the center. This agrees well with experimental results where the radial void fraction profile for bubble flow was measured using local probes (e.g. Kamp *et al.* 1993).

At $1 - g$, Kamp *et al.* (1993) found that the peak in the void fraction profile occurred at a distance from the wall equal to approximately one bubble diameter. They also found that the peak void fraction near the wall was much higher, relative to the void fraction at the centerline, when the liquid velocity was significantly larger than the gas velocity.

An investigation into the development of the void fraction profile in a 38 mm, i.d. vertical tube for bubble flow was done and reported recently by Grossetête (1995). Water–air mixtures were used with local measurements taken at $L/D$ locations of 8, 55 and 155 from the mixer. Grossetête (1995) found that there was a dominant 'saddle' shape profile at $L/D = 8$. This profile diminished as the $L/D$ ratio increased, mainly due to gas expansion and coalescence. At $L/D = 55$, the 'saddle' shape was still evident, however the void fraction at the center had also increased. At $L/D = 155$, the void fraction was highest at the center of the tube. Corresponding to the change in the void fraction profile, Grossetête (1995) found that the fluid velocity profile also changed. As the $L/D$ ratio increased, the fluid velocity profile became more of a parabolic shape. The increase in the

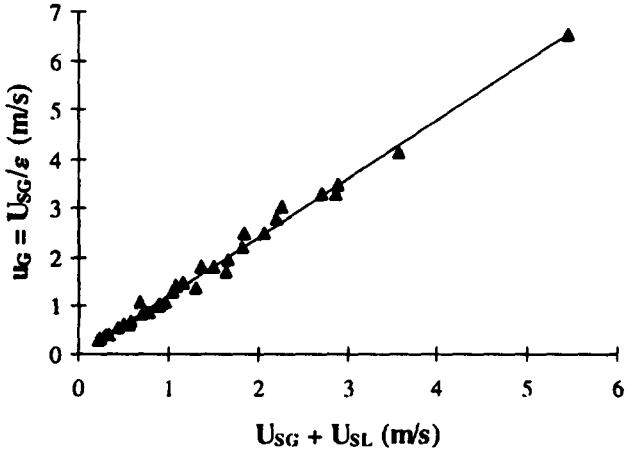


Figure 14. Results for slug flow at $1 - g$, $C_0 = 1.17$.

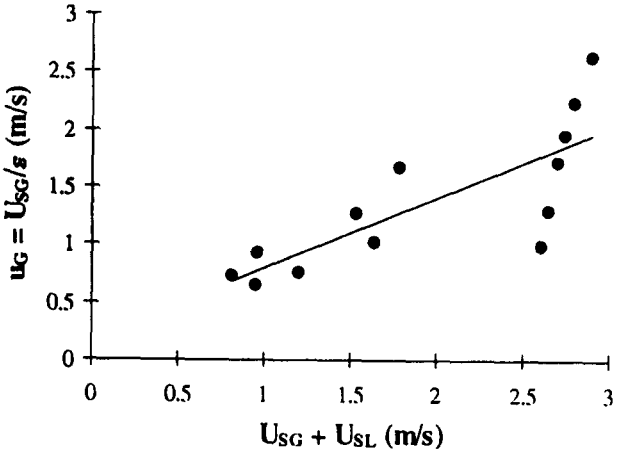


Figure 15. Bubbly flow at $1-g$, $C_0 = 0.61$.

radial velocity gradient, combined with the expanding gas, a higher coalescence rate and added turbulence, cause the void fraction to increase at the centerline. In the present study the void fraction sensor was located at $L/D = 65.1$. Therefore a value of $C_0 = 0.61$, which was obtained during ground tests, is in good agreement with the results of Grossetête (1995).

By comparing $C_0$ for the flight and ground data, it can be seen that the distribution coefficient is higher for $\mu - g$ than for $1 - g$. This suggests that the void fraction distribution at $\mu - g$ tends to be maximum at the centerline, as opposed to near the wall (conditions which are very common at $1 - g$). The other interesting observation is that under $\mu - g$ conditions, $C_0$ is the same for bubble and slug flows. This could be explained primarily in terms of the slip velocity. Since at $\mu - g$ the slip velocity is so small (almost zero), the difference between the two regimes should be also very small. For the $1 - g$ case, on the other hand, a change in the flow regime results in a change in $C_0$ since the void fraction profile and the velocity profile are different for different flow regimes. Drift velocity should also change for each flow regime since it depends on the momentum transfer between the two phases, and the shear stress due to interfacial interaction between the phases.

## 7. CONCLUSIONS

Using the capacitive method, void fraction measurements were obtained for water–air data collected at $1 - g$ and $\mu - g$. The data was collected for flow in a vertical 9.53 mm, i.d. tube over a wide range of liquid and gas flow rates, covering a range of void fraction from approximately 0.10–0.90. Comparisons were made between the void fraction results collected at $1 - g$ and $\mu - g$ and the Zuber and Findlay (1965) model. The following is a summary of the results:

(1) In comparing the average void fraction obtained for the bubble flow regime at $1 - g$ and $\mu - g$, it was found that for $\epsilon < 0.16$ and $U_{SG}/U_{SL} < 0.1$, the $\mu - g$ void fraction was approximately 8–25% higher. This could be attributed to a significant reduction in the slip velocity between the phases, as well as the greater influence of surface tension under reduced gravity. For $0.16 < \epsilon < 0.2$, the difference decreases until the trend is reversed with the $1 - g$ data slightly higher; approximately 7–16% higher.

(2) The overall average void fraction values for slug flow were found to be approximately 10% higher at $\mu - g$ compared to $1 - g$.

(3) The average values of void fraction for the transitional flow (slug–annular, and churn flows), at $\mu - g$ and $1 - g$ were found to be similar. The similarities in the average void fraction values could be attributed to the fact that inertia forces are becoming more dominant in this region.

(4) As with transitional flow, the average values of void fraction for annular flow, both at $1 - g$ and $\mu - g$, were also similar. The percent difference in the void fractions was within the uncertainty

of the measurements. Similar void fraction values would be expected since the flow is primarily dominated by inertia forces.

(5) The distribution coefficient, $C_0$, was determined to be 1.25 for the bubble and slug flows at $\mu - g$. For the bubble flow regime at $1 - g$, $C_0$ was less than 1.0, indicating a higher concentration near the wall. This agrees well with the typical 'saddle' shape void fraction profile present in vertical upward bubble flow at $1 - g$. For slug flow at $1 - g$, $C_0$ was found to be 1.17.

## REFERENCES

Albouelwafa, M. S. A. and Kendall, E. J. M. (1979) Analysis and design of helical capacitance sensors for volume fraction determination. *Rev. Sci. Instrum.* **50,** 872–878.

Bousman, S. (1995) Studies of two-phase gas–liquid flow in microgravity. NASA Contractor Report 19534.

Elkow, K. J. (1996) Void fraction measurement and analysis at normal gravity and microgravity conditions. M.Sc. thesis, Saskatoon, University of Saskatchewan.

Elkow, K. J. and Rezkallah, K. S. (1996) Void fraction measurements in gas–liquid flows using capacitance sensors. *Meas. Sci. Technol.* **7,** 1153–1163.

Grossetête, C. (1995) Experimental investigation and preliminary numerical simulations of void profile development in a vertical cylindrical pipe. *Proceedings of The 2nd International Conference on Multiphase Flow '95*—Kyoto, Japan, 3–7 April.

Huang, S. M., Stott, A. L., Green, R. G. and Beck, M. S. (1988) Electronic transducers for industrial measurement of low value capacitances. *J. Phys. E: Sci. Instrum.* **21,** 242–250.

Kamp, A., Colin, C. and Fabre, J. (1993) Bubbly flow in a pipe: influence of gravity upon void and velocity distributions. *3rd World Conference on Experimental Heat Transfer, Fluid Mechanics and Thermodynamics*, Honolulu, Hawaii, 30 October–5 November.

Li, H., Zhou, Z. and Hu, C. (1992) Measurement and evaluation of two-phase flow parameters. *IEEE Transactions on Instrum. and Meas.* **41,** 298–303.

Masuda, Y., Nishikawa, M. and Ichijo, B. (1980) New methods of measuring capacitance and resistance of very high loss materials at high frequencies. *IEEE Transactions on Instrum. and Meas.* **IM-29**, 28–36.

Shu, M. T., Winberger, C. B. and Lee, Y. H. (1982) A simple capacitance sensor for void fraction measurement in two-phase flow. *Ind. Eng. Chem. Fundam.* **21,** 175–181.

Zuber, N. and Findlay, J. A. (1965) Average volumetric concentration in two-phase flow systems. *Journal of Heat Transfer, Trans. ASME, Series C* **87,** 453–468.